INTERNATIONAL JOURNAL FOR NUMERICAL METHODS IN FLUIDS, VOL. 9, 1011–1024 (1989)

ON TVD DIFFERENCE SCHEMES FOR THE THREE-DIMENSIONAL EULER EQUATIONS IN GENERAL CO-ORDINATES

YOKO TAKAKURA

Scientific Systems Department, Fujitsu Limited, 1-17-25, Shinkamata, Otaku, Tokyo 144, Japan

AND

TOMIKO ISHIGURO AND SATORU OGAWA

National Aerospace Laboratory, 7-44-1 Jindaiji-Higashimachi, Chofushi, Tokyo 182, Japan

SUMMARY

An improved treatment for the Harten–Yee and Chakravarthy–Osher TVD numerical flux functions in general co-ordinates is presented. The proposed formulation is demonstrated by a series of numerical experiments for three-dimensional flows around the ONERA-M6 wing. The numerical results indicate that it is important to use a suitable artificial compression parameter in order to obtain more accurate solutions around the leading edge of the wing. The two TVD numerical fluxes give excellent results: they capture the shock wave without numerical oscillations, they capture the rapid expansion around the leading edge sharply, they have self-adjusting mechanisms regarding numerical viscosity and they also have robustness.

KEY WORDS Inviscid flow TVD difference scheme Shock wave Expansion wave

INTRODUCTION

The search for better schemes in computational fluid dynamics is continually evolving. First low-order-accurate upwind schemes were presented and then higher-order-accurate upwind schemes were proposed. The most recent notable improvements in numerical techniques are the development of high-order-accurate non-oscillatory shock capturing schemes such as total variation diminishing (TVD) schemes,[1] uniformly high-order-accurate non-oscillatory (UNO) schemes[2] and uniformly high-order-accurate essentially non-oscillatory (ENO) schemes.[3] Of the three, TVD schemes have already been applied to multidimensional complex fluid flow problems.

In addition, supercomputers with very fast operational processors and large memory have recently been developed and, as a result, three-dimensional flows around simple configurations have been numerically solved without difficulty. However, the need to seek better schemes still exists in order to capture shock waves and rapid expansions more sharply, to calculate hypersonic flows more accurately, to clarify turbulent phenomena, and so on.

Our interest in this paper is in the evaluation of TVD schemes for the three-dimensional Euler equations in general co-ordinates, with emphasis on their application to more practical flow problems. Two TVD schemes made practicable by Yee and Harten[4,5] and Chakravarthy and Osher[6] are chosen. These two algorithms differ in their methods of achieving higher-than-first-order TVD schemes.

0271–2091/89/081011–14$07.00

Received 7 December 1987
Revised 22 July 1988

There are three methods of applying TVD numerical fluxes to the flow problem in multi-dimensional general co-ordinates: the finite difference method (FDM), the finite element method (FEM) and the finite volume method (FVM) (a special version of FEM). FVM departs from FDM mainly in three-dimensional applications. Within FDM formulations there are many variations. In Reference 7 we suggested a different method of evaluating the numerical fluxes for the Harten–Yee and the Chakravarthy–Osher schemes in generalized co-ordinates by use of FDM. From the flow fields presented in Reference 7 we prefer our approach over the original formulation.

This paper is intended to confirm the basis of improvements in our earlier work[7] with more extensive numerical experiments towards the practical use of TVD–FDMs.

GOVERNING EQUATIONS

The independent variables in Cartesian co-ordinates are denoted by

$$(t, x_k), \quad k = 1, 2, 3, \tag{1}$$

and those in general co-ordinates are denoted by

$$(\tau, \xi^l), \quad l = 1, 2, 3. \tag{2}$$

The three-dimensional Euler equations in Cartesian co-ordinates in conservative form

$$\frac{\partial \mathbf{Q}}{\partial t} + \frac{\partial \mathbf{F}_k}{\partial x_k} = \mathbf{0}, \tag{3}$$

where

$$\mathbf{F}_k = \mathbf{F}_k(\mathbf{Q}), \tag{4}$$

are transformed into the conservation law in general co-ordinates

$$\frac{\partial \hat{\mathbf{Q}}}{\partial \tau} + \frac{\partial \hat{\mathbf{F}}^l}{\partial \xi^l} = \mathbf{0}, \tag{5}$$

with a transformation of variables

$$\tau = t, \qquad \xi^l = \xi^l(t, x_1, x_2, x_3), \tag{6}$$

where

$$\hat{\mathbf{Q}} = \mathbf{Q}/J, \tag{7a}$$

$$\hat{\mathbf{F}}^l = (\xi^l_t/J)\mathbf{Q} + (\xi^l_{x_k}/J)\mathbf{F}_k \tag{7b}$$

and J is the Jacobian of transformation. Here the subscript and superscript indicate the variables in Cartesian and general co-ordinates respectively and $\hat{}$ denote the variables multiplied by $1/J$. It is apparent from equations (4) and (7b) that the flux in the general co-ordinates, $\hat{\mathbf{F}}^l$, is a function of $\mathbf{Q}$ and metrics,

$$\hat{\mathbf{F}}^l = \hat{\mathbf{F}}^l(\mathbf{Q}, \xi^l_t/J, \xi^l_{x_1}/J, \xi^l_{x_2}/J, \xi^l_{x_3}/J); \tag{8}$$

and the conventional notation that the flux $\hat{\mathbf{F}}^l$ is a function of $\hat{\mathbf{Q}}$ alone,

$$\hat{\mathbf{F}}^l = \hat{\mathbf{F}}^l(\hat{\mathbf{Q}}), \tag{9}$$

is not a precise expression.

Here, as a preliminary to applying TVD–FDMs to the conservation law system (5), some definitions for notation are described: for the Jacobian matrix,

$$\mathbf{A}^{\iota} \equiv \frac{\partial \mathbf{F}^{\iota}}{\partial \mathbf{Q}} \left(= \frac{\partial \hat{\mathbf{F}}^{\iota}}{\partial \hat{\mathbf{Q}}} \right), \tag{10}$$

where $\mathbf{F}^{\iota}$ is the flux in general co-ordinates not multiplied by $1/J$, and for the similarity transformation to diagonalize it,

$$\mathbf{A}^{\iota} = \mathbf{R}^{\iota} \mathbf{\Lambda}^{\iota} (\mathbf{R}^{\iota})^{-1}, \qquad \mathbf{\Lambda}^{\iota} = \operatorname{diag}[(a^{\iota})^{m}], \tag{11}$$

where $(a^{\iota})^{m}$ ($m = 1$–5) are the eigenvalues of matrix $\mathbf{A}^{\iota}$. The elements of these matrices are fully described in Reference 8. (In our notation $\mathbf{A}^1$, $\mathbf{A}^2$ and $\mathbf{A}^3$ are equivalent to $\hat{\mathbf{A}}$, $\hat{\mathbf{B}}$ and $\hat{\mathbf{C}}$ in their notation respectively.)

TVD DIFFERENCE SCHEMES

TVD numerical fluxes in general co-ordinates

Generally the numerical flux function of TVD schemes can be written as

$$\tilde{\mathbf{F}}^{\iota}_{i_{\iota}+1/2} = (1/2)[\hat{\mathbf{F}}^{\iota}_{i_{\iota}} + \hat{\mathbf{F}}^{\iota}_{i_{\iota}+1} + \Delta\bar{\mathbf{F}}^{\iota}_{i_{\iota}+1/2}], \tag{12}$$

where $\Delta\bar{\mathbf{F}}^{\iota}$ is added to achieve the TVD property and is evaluated by

$$|\Delta\bar{\mathbf{F}}^{\iota}| \sim \left| \frac{\partial \hat{\mathbf{F}}^{\iota}}{\partial \xi^{\iota}} \Delta\xi^{\iota} \right|, \tag{13}$$

and subscript i_{ι} has the following meanings:

$$i_{\iota} = \begin{cases} i & \text{for } \iota = 1, \\ j & \text{for } \iota = 2, \\ k & \text{for } \iota = 3. \end{cases} \tag{14}$$

Our modification in Reference 7 is mainly concerned with the evaluation of $\Delta\bar{\mathbf{F}}^{\iota}$.

In a series of extensions of TVD–FDMs from single conservation law to a system in general co-ordinates,[5,9] the mathematically non-exact relation which was probably induced by equation (9),

$$\frac{\partial \hat{\mathbf{F}}^{\iota}}{\partial \xi^{\iota}} \neq \frac{\partial \hat{\mathbf{F}}^{j}}{\partial \hat{\mathbf{Q}}} \frac{\partial \hat{\mathbf{Q}}}{\partial \xi^{j}} = \mathbf{A}^{j} \frac{\partial \hat{\mathbf{Q}}}{\partial \xi^{j}}, \tag{15}$$

has been used, and with the local linearization in space the flux divergence is expanded as follows:

$$\frac{\partial \hat{\mathbf{F}}^{\iota}}{\partial \xi^{\iota}} \sim \mathbf{R}^{\iota} \mathbf{\Lambda}^{\iota} (\mathbf{R}^{\iota})^{-1} \frac{\partial \hat{\mathbf{Q}}}{\partial \xi^{\iota}} \sim \mathbf{R}^{\iota} \mathbf{\Lambda}^{\iota} \frac{\partial}{\partial \xi^{\iota}} \{(\mathbf{R}^{\iota})^{-1} \hat{\mathbf{Q}}\}. \tag{16}$$

On the other hand, the exact relation has been derived in Reference 7 as follows. Transforming the divergence of flux into the non-conservative form as[10]

$$\frac{\partial \hat{\mathbf{F}}^{\iota}}{\partial \xi^{\iota}} = (\xi^{j}_{t}/J) \frac{\partial \mathbf{Q}}{\partial \xi^{j}} + (\xi^{j}_{x_k}/J) \frac{\partial \mathbf{F}_k}{\partial \xi^{j}} \tag{17}$$

and applying the chain rule to $\partial \mathbf{F}_k(\mathbf{Q})/\partial \xi^{j}$ results in our basis

$$\frac{\partial \hat{\mathbf{F}}^{\iota}}{\partial \xi^{\iota}} = \frac{\partial \hat{\mathbf{F}}^{j}}{\partial \mathbf{Q}} \frac{\partial \mathbf{Q}}{\partial \xi^{j}} = \frac{1}{J} \mathbf{A}^{j} \frac{\partial \mathbf{Q}}{\partial \xi^{j}}, \tag{18}$$

and also the local linearization brings the following approximation:

$$\frac{\partial \hat{\mathbf{F}}^l}{\partial \xi^l} \sim \frac{1}{J}\mathbf{R}^l\mathbf{\Lambda}^l(\mathbf{R}^l)^{-1}\frac{\partial \mathbf{Q}}{\partial \xi^l} \sim \frac{1}{J}\mathbf{R}^l\mathbf{\Lambda}^l\frac{\partial}{\partial \xi^l}\{(\mathbf{R}^l)^{-1}\mathbf{Q}\}. \tag{19}$$

Note that the difference between the conventional expression (15) and our precise expression (18) lies in the treatment of the Jacobian: in equation (15) $1/J$ remains inside the differential operator, while in equation (18) $1/J$ is outside it. In Reference 7 the comparison between solutions based on the conventional treatment (16) and our modified treatment (19) is shown for the flow problem of a triple shock wave (weak and strong shock waves and united shock wave) around the ONERA-M6 wing; the conventional treatment captures only the strong shock wave but misses the weak shock wave near the leading edge where the change of metrics is large, while our modified treatment captures the triple shock wave clearly. Therefore our modified treatment (19) is used in this paper.

From equations (12), (13) and (19) the numerical flux function in general co-ordinates is described as

$$\tilde{\mathbf{F}}^l_{i_l+1/2} \equiv (1/2)[\hat{\mathbf{F}}^l_{i_l} + \hat{\mathbf{F}}^l_{i_l+1} + \{(1/J)\mathbf{R}^l\mathbf{\Phi}^l\}_{i_l+1/2}], \tag{20}$$

and the following two characteristic quantities can be substituted for the propagated quantity in the single scalar conservation law:

$$\alpha_v \equiv (\mathbf{R}^l)^{-1}_{i_l+1/2}\Delta_v\mathbf{Q}, \tag{21a}$$

$$\alpha_v \equiv (\mathbf{R}^l)^{-1}_{v}\Delta_v\mathbf{Q}, \tag{21b}$$

where v takes the values $i_l - 1/2$, $i_l + 1/2$ and $i_l + 3/2$, and

$$\Delta_{i_l+1/2}\mathbf{Q} = \mathbf{Q}_{i_l+1} - \mathbf{Q}_{i_l}. \tag{22}$$

Modified Harten–Yee TVD scheme. The second-order numerical flux function proposed by Yee and Harten[5] is used, with modification[7] based on the correct estimation (19), instead of using the straightforward extension based on equation (16). The elements of $\mathbf{\Phi}^l$ denoted by ϕ^m are

$$\phi^m_{i_l+1/2} \equiv (1/2)\psi(a^{lm}_{i_l+1/2})(g^m_{i_l} + g^m_{i_l+1}) - \psi(a^{lm}_{i_l+1/2} + \gamma^m_{i_l+1/2})\alpha^m_{i_l+1/2}, \tag{23}$$

with the adjustment quantity for high accuracy $g^m_{i_l}$ defined by

$$g^m_{i_l} = \text{minmod}[\alpha^m_{i_l-1/2}, \alpha^m_{i_l+1/2}], \tag{24}$$

the function ψ containing the entropy condition

$$\psi(z) = \begin{cases} |z| & |z| \geqslant \varepsilon \\ (z^2+\varepsilon^2)/2\varepsilon, & |z| \leqslant \varepsilon, \end{cases} \tag{25}$$

and

$$\gamma^m_{i_l+1/2} = (1/2)\psi(a^{lm}_{i_l+1/2})\begin{cases} (g^m_{i_l+1} - g^m_{i_l})/\alpha^m_{i_l+1/2} & \alpha^m_{i_l+1/2} \neq 0, \\ 0 & \alpha^m_{i_l+1/2} = 0. \end{cases} \tag{26}$$

Here we use the definition (21b) for α, and the only difference between the current formulation and the original one[5] is the evaluated point (subscript) of the Jacobian in the adjustment quantity for high accuracy.

Further, in order to make the shock waves clearer, the artificial compression,[4] which is important in TVD schemes, is imposed by using the following $\tilde{g}_{i_l}$ instead of g_{i_l}:

$$\tilde{g}_{i_l} = (1 + \omega\theta_{i_l})g_{i_l}, \quad \omega > 0, \tag{27}$$

$$\theta_{i_l} = \frac{|\Delta_{i_l+1/2}\mathbf{Q} - \Delta_{i_l-1/2}\mathbf{Q}|}{|\Delta_{i_l+1/2}\mathbf{Q}| + |\Delta_{i_l-1/2}\mathbf{Q}|}, \tag{28}$$

where ω is a compression parameter.

Modified Chakravarthy–Osher TVD scheme. The high-accuracy numerical flux proposed by Chakravarthy and Osher[6] is

$$\begin{aligned}\mathbf{\Phi}^l_{i_l+1/2} = &-(\boldsymbol{\sigma}^+_{i_l+1/2} - \boldsymbol{\sigma}^-_{i_l+1/2}) \\ &- \{(1-\phi)/2\}\bar{\boldsymbol{\sigma}}^-_{i_l+3/2} - \{(1+\phi)/2\}\bar{\boldsymbol{\sigma}}^-_{i_l+1/2} \\ &+ \{(1+\phi)/2\}\bar{\boldsymbol{\sigma}}^+_{i_l+1/2} + \{(1-\phi)/2\}\bar{\boldsymbol{\sigma}}^+_{i_l-1/2},\end{aligned} \tag{29}$$

where ϕ is a parameter to control the accuracy of the scheme. We use the third order ($\phi = 1/3$). Our modified form[8] in the general co-ordinate system for $\boldsymbol{\sigma}^{\pm}$ and flux-limited values $\bar{\boldsymbol{\sigma}}^{\pm}$ and $\bar{\boldsymbol{\sigma}}^{\pm}$ is as follows:

$$\boldsymbol{\sigma}^{\pm}_{\nu} = \mathbf{\Lambda}^{\pm}_{i_l-1/2}\alpha_{\nu}, \quad \text{for } \nu = i_l - 1/2,\ i_l + 1/2,\ i_l + 3/2, \tag{30}$$

$$\bar{\boldsymbol{\sigma}}^-_{i_l+3/2} = \text{minmod}[\boldsymbol{\sigma}^-_{i_l+3/2},\ \beta\boldsymbol{\sigma}^-_{i_l+1/2}], \tag{31a}$$

$$\bar{\boldsymbol{\sigma}}^-_{i_l+1/2} = \text{minmod}[\boldsymbol{\sigma}^-_{i_l+1/2},\ \beta\boldsymbol{\sigma}^-_{i_l+3/2}], \tag{31b}$$

$$\bar{\boldsymbol{\sigma}}^+_{i_l+1/2} = \text{minmod}[\boldsymbol{\sigma}^+_{i_l+1/2},\ \beta\boldsymbol{\sigma}^+_{i_l-1/2}], \tag{31c}$$

$$\bar{\boldsymbol{\sigma}}^+_{i_l-1/2} = \text{minmod}[\boldsymbol{\sigma}^+_{i_l-1/2},\ \beta\boldsymbol{\sigma}^+_{i_l+1/2}], \tag{31d}$$

where

$$\mathbf{\Lambda}^{\pm} = (\mathbf{\Lambda} \pm |\mathbf{\Lambda}|)/2 \tag{32}$$

and β is a compression parameter determined in the range given by

$$1 < \beta \leqslant \frac{3-\phi}{1-\phi}. \tag{33}$$

Here we use the definition (21a) for α, and the only difference between the current formulation and the original one[6] is the evaluated point (subscript) of the locally fixed coefficient $(1/J)\,\mathbf{A}^l$ in the quantity added for high accuracy.

Left-hand-side operator

A one-parameter family of explicit and implicit TVD schemes[4,5] can be written as

$$\begin{aligned}&\delta\hat{\mathbf{Q}}^n_{i,j,k} + \lambda^1\theta[(\tilde{\mathbf{F}}^1)^{n+1}_{i+1/2,j,k} - (\tilde{\mathbf{F}}^1)^{n+1}_{i-1/2,j,k}] + \lambda^2\theta[(\tilde{\mathbf{F}}^2)^{n+1}_{i,j+1/2,k} - (\tilde{\mathbf{F}}^2)^{n+1}_{i,j-1/2,k}] \\ &\quad + \lambda^3\theta[(\tilde{\mathbf{F}}^3)^{n+1}_{i,j,k+1/2} - (\tilde{\mathbf{F}}^3)^{n+1}_{i,j,k-1/2}] \\ &= -\lambda^1(1-\theta)[(\tilde{\mathbf{F}}^1)^n_{i+1/2,j,k} - (\tilde{\mathbf{F}}^1)^n_{i-1/2,j,k}] - \lambda^2(1-\theta)[(\tilde{\mathbf{F}}^2)^n_{i,j+1/2,k} - (\tilde{\mathbf{F}}^2)^n_{i,j-1/2,k}] \\ &\quad - \lambda^3(1-\theta)[(\tilde{\mathbf{F}}^3)^n_{i,j,k+1/2} - (\tilde{\mathbf{F}}^3)^n_{i,j,k-1/2}],\end{aligned} \tag{34}$$

where

$$\delta\hat{\mathbf{Q}}^n = \hat{\mathbf{Q}}^{n+1} - \hat{\mathbf{Q}}^n, \tag{35}$$

$$\lambda^l = \Delta t/\Delta\xi^l \tag{36}$$

and θ is a parameter; equation (34) with $\theta = 0$ is an explicit scheme and with $\theta \neq 0$ is an implicit scheme.

The flux on the left-hand side is linearized in time as follows:

$$(\tilde{\mathbf{F}}^l)^{n+1} \sim (\tilde{\mathbf{F}}^l)^n + \Delta\tilde{\mathbf{F}}^l, \tag{37a}$$

$$\Delta\tilde{\mathbf{F}}^l = (\partial\tilde{\mathbf{F}}^l/\partial\mathbf{Q})^n \delta\mathbf{Q}^n = (\partial\tilde{\mathbf{F}}^l/\partial\hat{\mathbf{Q}})^n \delta\hat{\mathbf{Q}}^n, \tag{37b}$$

and this relation is reasonable when the grid is still. If a moving grid is used, this relation no longer holds good because of equation (8). In this paper the case of a stationary grid is considered. When $(\tilde{\mathbf{F}}^l)^n$ is moved to the right-hand side in equation (34), $\Delta\tilde{\mathbf{F}}^l$ is left on the left-hand side. For the left-hand side the numerical flux function for the first order is used and is written by equation (20) with

$$\mathbf{\Phi}^l_{i_l+1/2} = -|\mathbf{\Lambda}^l_{i_l+1/2}|\alpha_{i_l+1/2} \tag{38}$$

if the entropy condition is excluded.

From the above, either operator solving $\delta\mathbf{Q}^n$ or $\delta\hat{\mathbf{Q}}^n$ can be constituted. Here the latter, the conventional one of Yee and Harten,[5] is used for convenience, since the left-hand-side operator can be considered only as a tool to reach the steady state, the right-hand side. The conventional implicit operator is the same as the result of the next approximation for the numerical viscosity:

$$\{(1/J)\mathbf{R}^l\mathbf{\Phi}^l\}_{i_l+1/2} = -[(1/J)\mathbf{R}^l|\mathbf{\Lambda}^l|(\mathbf{R}^l)^{-1}]_{i_l+1/2}\Delta_{i_l+1/2}\mathbf{Q} \tag{39a}$$

$$\sim -\{(1/J)\mathrm{diag}[\max_m|(a^l)^m|\}_{i_l+1/2}\Delta_{i_l+1/2}\mathbf{Q} \tag{39b}$$

$$\sim -\{\mathrm{diag}[\max_m|(a^l)^m|]\}_{i_l+1/2}\Delta_{i_l+1/2}\hat{\mathbf{Q}}. \tag{39c}$$

Although the approximation (39c) is equivalent to the use of the non-exact relation (15), it does not induce large error in the two-point numerical flux for the first order. Moreover, since the left-hand-side operator is less than first-order accurate if using the approximation (39b), equation (39c) matters little. Locally linearizing the coefficients of equation (39c), applying equation (37b) and further adopting an ADI form results in the LCI (linearized conservative implicit)–ADI form[5]

$$\begin{aligned}
&[\mathbf{I} + \lambda^1\theta\mathbf{H}^1_{i+1/2,j,k} - \lambda^1\theta\mathbf{H}^1_{i-1/2,j,k}][\mathbf{I} + \lambda^2\theta\mathbf{H}^2_{i,j+1/2,k} - \lambda^2\theta\mathbf{H}^2_{i,j-1/2,k}] \\
&\quad\times[\mathbf{I} + \lambda^3\theta\mathbf{H}^3_{i,j,k+1/2} - \lambda^3\theta\mathbf{H}^3_{i,j,k-1/2}]\delta\hat{\mathbf{Q}}^n \\
&= -\{\lambda^1[\tilde{\mathbf{F}}^{1n}_{i+1/2,j,k} - \tilde{\mathbf{F}}^{1n}_{i-1/2,j,k}] + \lambda^2[\tilde{\mathbf{F}}^{2n}_{i,j+1/2,k} - \tilde{\mathbf{F}}^{2n}_{i,j-1/2,k}] \\
&\quad+ \lambda^3[\tilde{\mathbf{F}}^{3n}_{i,j,k+1/2} - \tilde{\mathbf{F}}^{3n}_{i,j,k-1/2}]\},
\end{aligned} \tag{40}$$

where

$$\mathbf{H}^l_{i_l\pm1/2} = (1/2)(\mathbf{A}^l_{i_l\pm1} + \mathbf{\Omega}^l{}_{i_l\pm1/2})^n, \tag{41}$$

$$\mathbf{\Omega}^l{}_{i_l\pm1/2} = -\{\mathrm{diag}[\max_m|(a^l)^m|]\}_{i_l+1/2}\Delta_{i_l+1/2}, \tag{42}$$

with the non-standard notation

$$\mathbf{H}^l_{i_l\pm1/2}\delta\hat{\mathbf{Q}} = (1/2)[(\mathbf{A}^l\delta\hat{\mathbf{Q}})_{i_l\pm1} + \mathbf{\Omega}^l{}_{i_l\pm1/2}\delta\hat{\mathbf{Q}}]. \tag{43}$$

For the steady state—the right-hand side in equation (40)—which should be evaluated more carefully, our modified Harten–Yee and Chakravarthy–Osher numerical fluxes are used.

RESULTS AND DISCUSSION

Conditions for numerical experiments

The modified Harten–Yee TVD scheme and the modified Chakravarthy–Osher scheme are used for numerical experiments, and for comparison the Beam–Warming scheme[11] improved by Pulliam and Steger[12] is adopted. In order to improve the convergence rate to the steady state, we apply the diagonalization of the ADI operator[8] and the local time stepping[12] $\Delta t = \Delta t_{\text{ref}}/(1 + J^{1/3})$ to the three schemes mentioned above. Treatments of the boundary conditions are almost the same as those by Pulliam and Steger.[12] For the treatment of five-point TVD schemes over boundaries, the zeroth-order extrapolation for the physical value of $\mathbf{Q}$ is adopted.[7] Roe's average[13] is used here to evaluate the physical values at the midpoint $i + 1/2$, although no difference is observed between solutions by Roe's average and solutions by the arithmetic average.

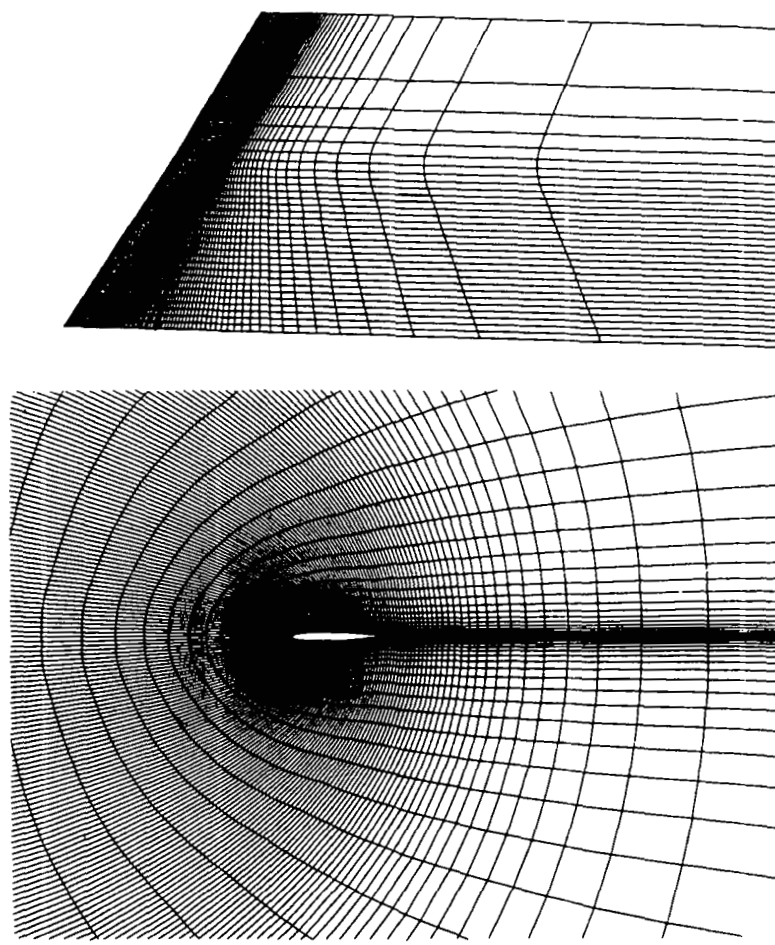

Figure 1. Grid view around ONERA-M6 wing

The numerical experiments are carried out for the ONERA-M6 wing. Three kinds of flow problems are solved: case 1, $M_\infty = 0{\cdot}8398$, $\alpha = 1{\cdot}07°$; case 2, $M_\infty = 0{\cdot}8395$, $\alpha = 3{\cdot}06°$; case 3, $M_\infty = 0{\cdot}8372$, $\alpha = 6{\cdot}07°$; where M_∞ is the freestream Mach number and α is the angle of attack. In this sequence a triple shock wave becomes stronger in the experimental data.[14]

The grid used in our numerical experiments is of the C–H type, generated by the combination of conformal mappings and shearing transformations.[15] Figure 1 shows the grid distribution around the wing. The number of grid points is 191 × 33 × 24, the minimum grid cell length on the wing is 0·01 and the semi-span length is 1·0.

Comparison of computing times

Table I shows the ratio of computing times for the modified Harten–Yee TVD scheme, the modified Chakravarthy–Osher TVD scheme and the Beam–Warming scheme. For each TVD

Table I. Comparison of computing times

Yee–Harten		Chakravarthy–Osher		Beam–Warming
implicit	explicit	implicit	explicit	implicit
1·48	1·22	1·70	1·43	1·0

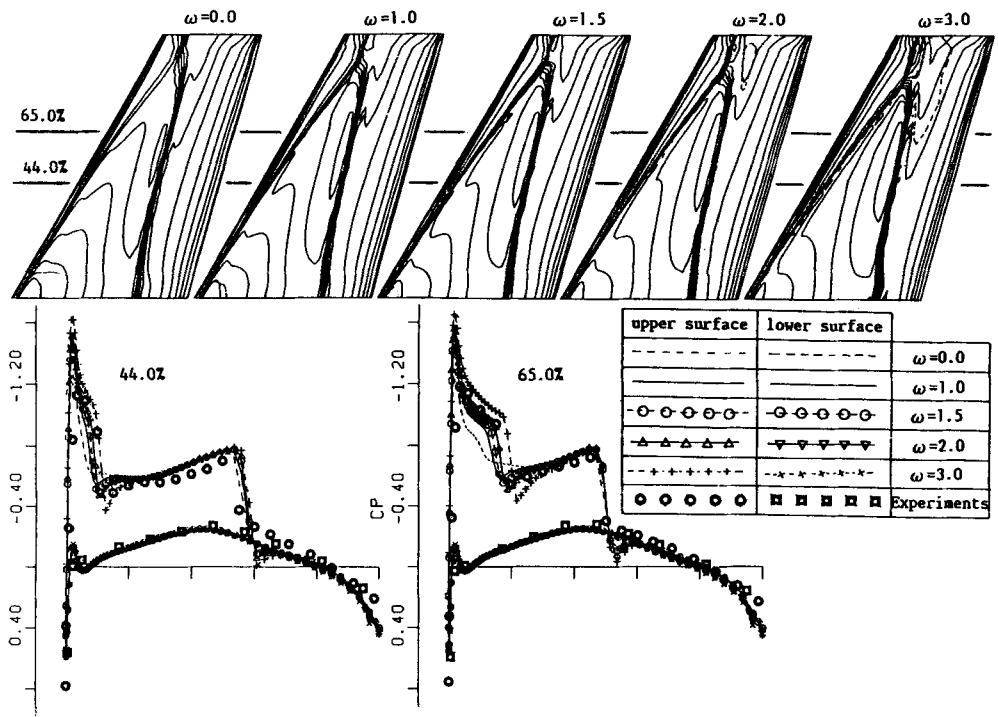

Figure 2. Change of solutions with compression parameter in case of Harten–Yee numerical flux ($M_\infty = 0{\cdot}8395$, $\alpha = 3{\cdot}06°$). Isobaric contours on upper wing surface and C_p distributions

scheme the explicit ($\theta = 0$ in equation (40)) and implicit ($\theta = 1$) methods are compared. These data were obtained on a VP-400 vector computer.

From the table the TVD schemes seem to be time-consuming, but this is a fairly minor issue because the computing time greatly depends on the coding technique. The more important point is that in the Beam–Warming scheme a process of trial and error is required to choose the proper values of the dissipation coefficient, while the TVD schemes have self-adjusting mechanisms (see later). Therefore the TVD schemes will consume less total computing time to accomplish good numerical simulation than the Beam–Warming scheme.

The maximum Courant numbers are about 1 and 20 for the explicit and implicit ($\Delta t_{\text{ref}} = 1$) methods respectively in case 2. Although higher Courant numbers can be obtained in the implicit methods by increasing Δt_{ref}, this does not improve the convergence rate very much.

For the computational cost to the steady state, the implicit methods ($\theta = 1$) are used in the following numerical experiments.

Numerical experiments for artificial compressions

Figures 2 and 3 show the solutions by the modified Harten–Yee scheme and the modified Chakravarthy–Osher scheme respectively when the value of the compression parameter is increased in case 2. With the Harten–Yee scheme the weak shock wave grows stronger and stronger with the increase in the compression parameter ω, while with the Chakravarthy–Osher scheme the weak shock wave grows stronger to some extent but does not grow beyond a certain limit with the increase in the compression parameter β. When the artificial compressions are not imposed ($\omega = 0$, $\beta = 1$), the two TVD solutions agree with each other (Figure 4).

When $\omega = 2$ is used, the weak shock wave in the case of the Harten–Yee scheme is located at almost the same position as that of the solution with maximum allowable compression value ($\beta = 4$) in the case of the Chakravarthy–Osher scheme, and the maximum allowable value of β satisfies the TVD property for a scalar hyperbolic conservation law. Consequently the compression parameters are fixed at the above values. These values are also recommended in References 4 and 6 respectively.

Comparison of schemes

Comparisons of solutions obtained by the modified Harten–Yee scheme, the modified Chakravarthy–Oscher scheme and the Beam–Warming scheme are shown in Figures 5, 6 and 7 for cases 1, 2 and 3 respectively. In a series of experiments it is observed that the triple shock wave grows stronger as the angle of attack is increased.

For cases 1–3 the following observations are made.

The two TVD schemes capture the strong shock wave and united shock wave without oscillations, while the Beam–Warming scheme produces some oscillations near the shock waves.

The two TVD schemes caputure the rapid expansion and weak shock wave around the leading edge much better than the Beam–Warming scheme. Both TVD schemes capture the rapid leading edge expansion more strongly than the experiments and this would be a good tendency in inviscid flows, while the Beam–Warming scheme injures the rapid expansion, particularly in case 3. According to Reference 16, the fourth-order dissipation term in the Beam–Warming scheme acts more than is needed at the rapid expansion and shock wave.

The difference in solutions between the two TVD schemes is that the modified Harten–Yee TVD scheme captures the leading edge expansion and weak shock waves more strongly than the modified Chakravarthy–Osher scheme. This discrepancy is due to the flux limiters and compression parameters.

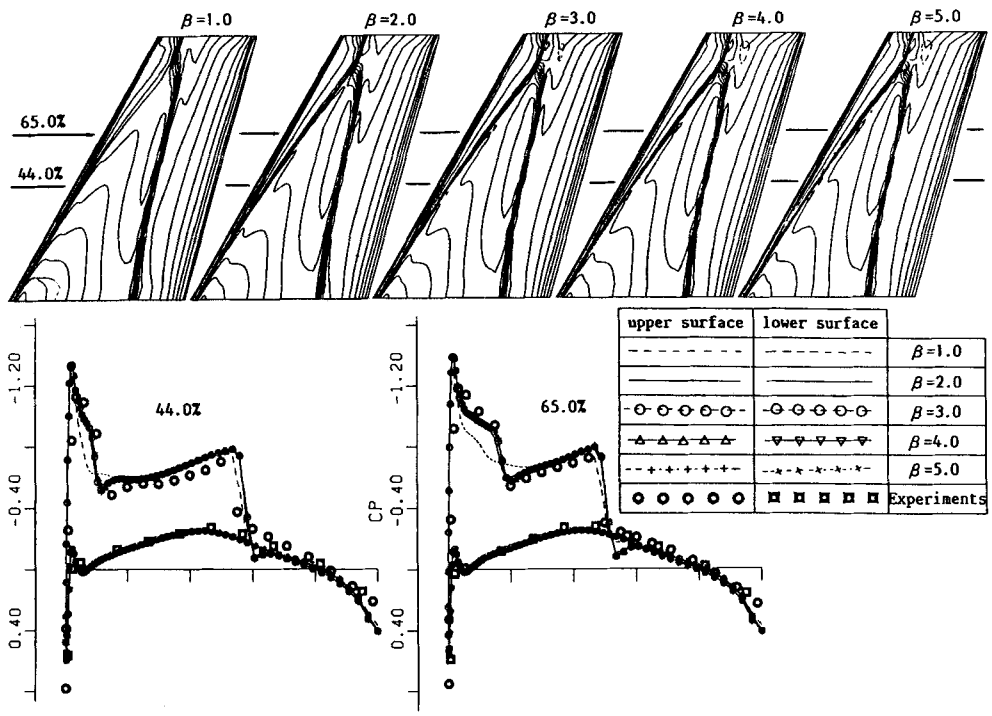

Figure 3. Change of solutions with compression parameter in case of Chakravarthy–Osher numerical flux ($M_\infty = 0{\cdot}8395$, $\alpha = 3{\cdot}06°$). Isobaric contours on upper wing surface and C_p distributions

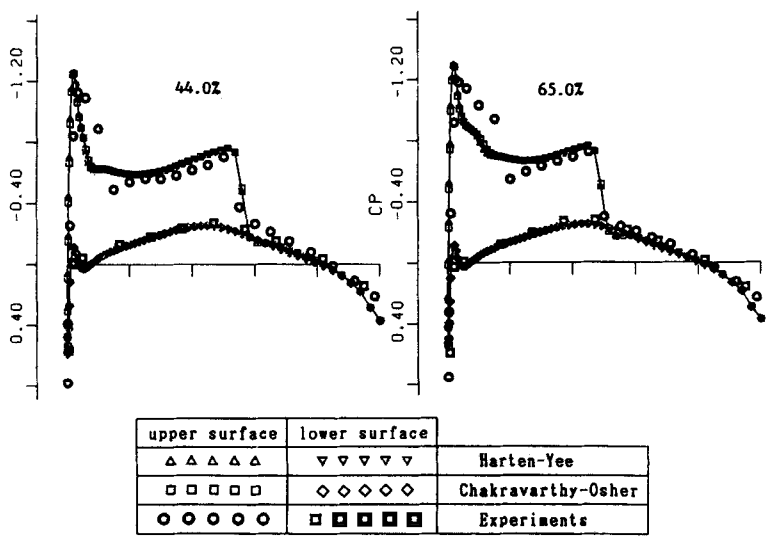

Figure 4. Comparisons of C_p distributions between Harten–Yee and Chakravarthy–Osher numerical fluxes with no compression ($M_\infty = 0{\cdot}8395$, $\alpha = 3{\cdot}06°$)

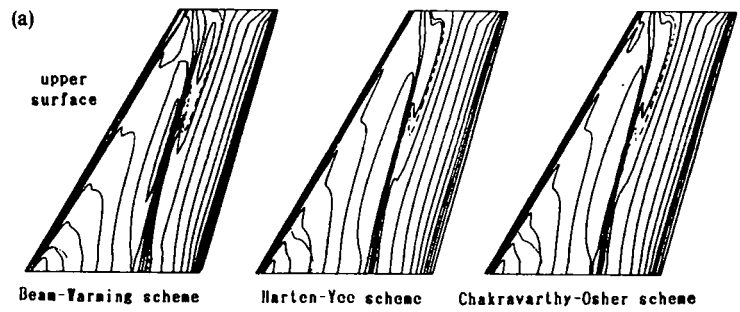

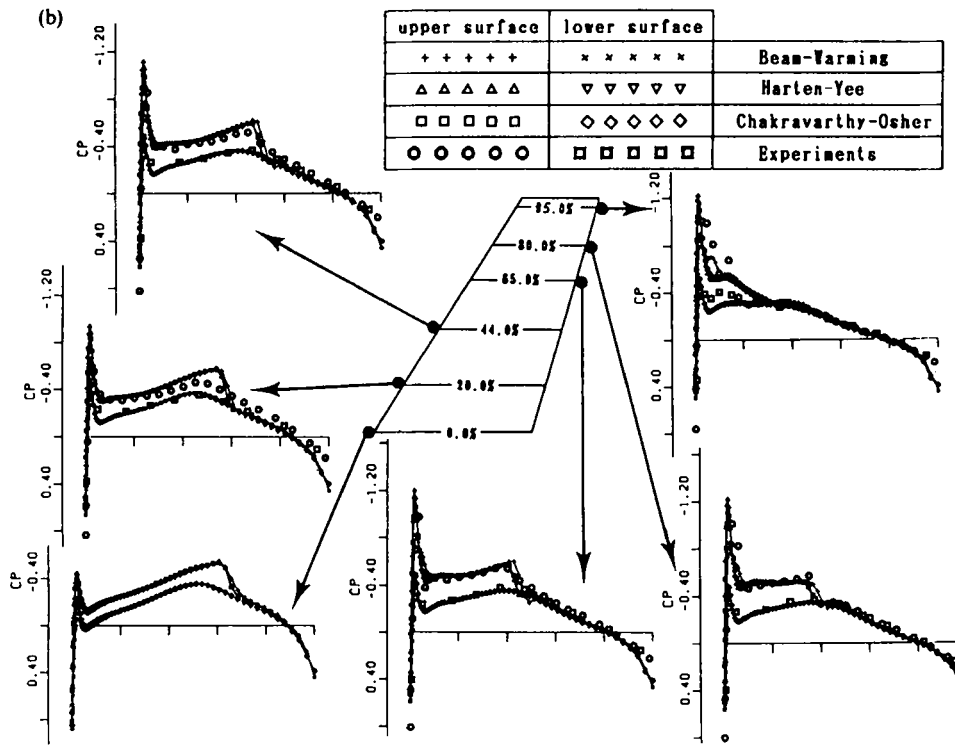

Figure 5. Comparisons of schemes ($M_\infty = 0{\cdot}8398$, $\alpha = 1{\cdot}07°$). (a) Isobaric contours on upper wing surface. (b) C_p distributions on wing surface

In a series of numerical experiments the value of the dissipation coefficient in the Beam–Warming scheme must be adjusted with the change of flow conditions and also with the change of grid fineness[7] in order to preserve solutions from high numerical oscillations and divergence, while the two TVD schemes have self-adjusting mechanisms with the fixed values of the compression parameters recommended earlier and have the property of robustness.

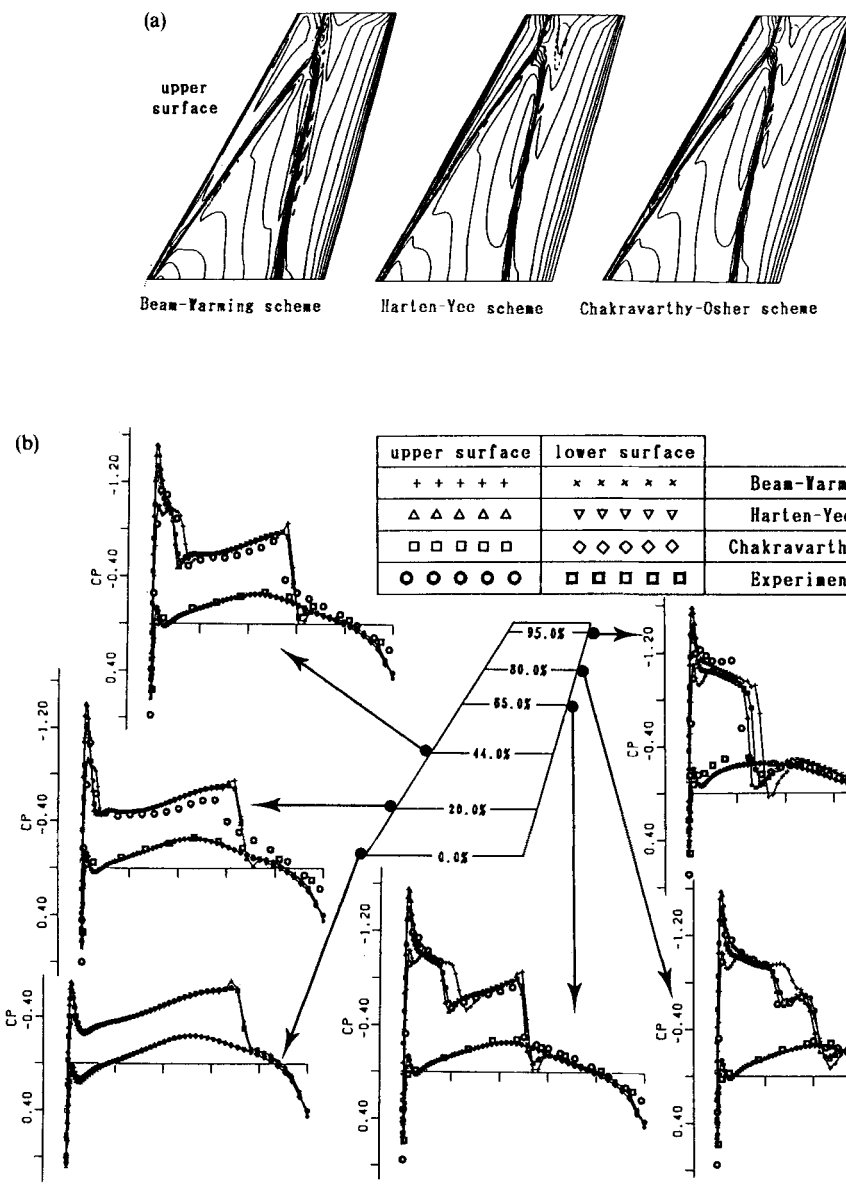

Figure 6. Comparisons of schemes ($M_\infty = 0{\cdot}8395$, $\alpha = 3{\cdot}06°$). (a) Isobaric contours on upper wing surface. (b) C_p distributions on wing surface

CONCLUSIONS

An improved treatment for the TVD numerical flux functions in general co-ordinates is presented in more detail than in our earlier paper.[7] This improvement affects the higher-order numerical flux function terms. Here the modifications for the Harten–Yee numerical flux and the Chakravarthy–Osher numerical flux are presented and applied to three-dimensional inviscid flows around the ONERA-M6 wing.

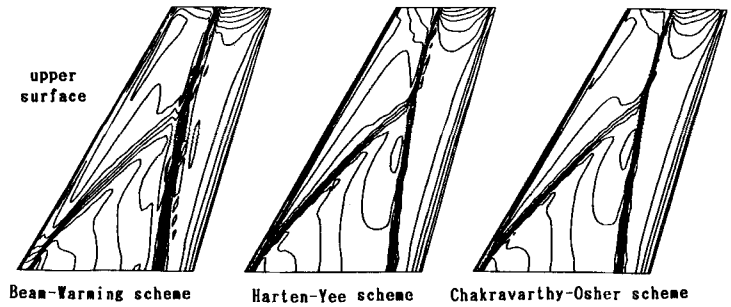

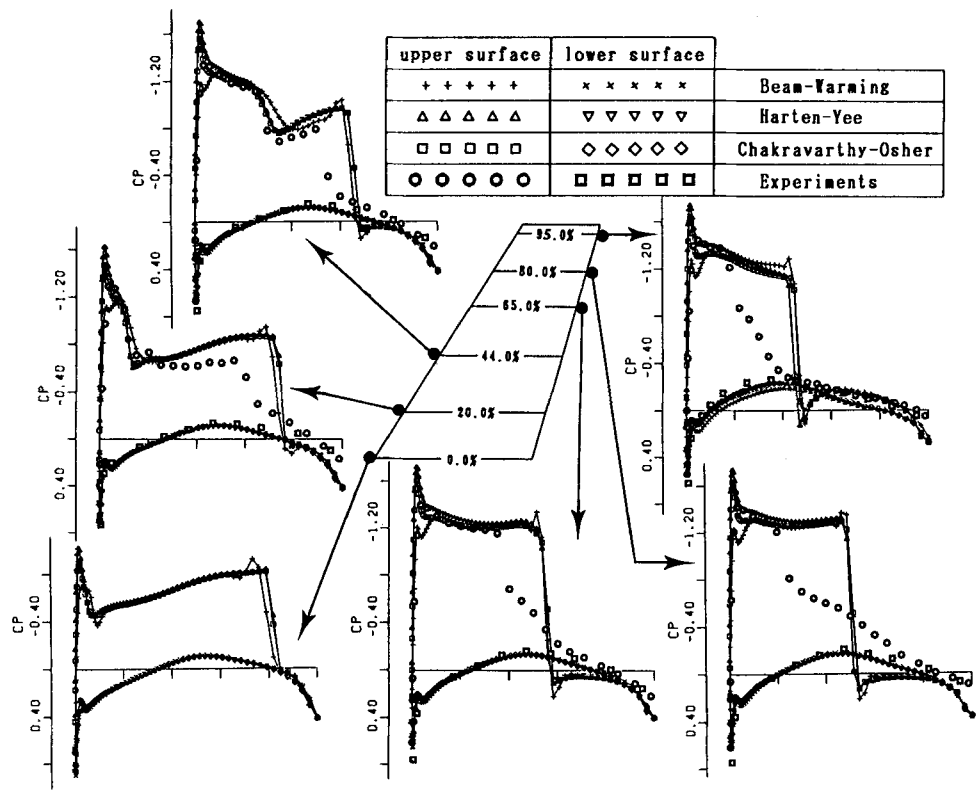

Figure 7. Comparisons of schemes ($M_\infty = 0{\cdot}8372$, $\alpha = 6{\cdot}07°$). (a) Isobaric contours on upper wing surface. (b) C_p distributions on wing surface

The numerical results indicate that it is important to use a suitable artificial compression parameter in order to obtain more accurate solutions around the leading edge of the wing.

The two TVD numerical fluxes give excellent results: they capture the shock wave without numerical oscillations, they capture the rapid expansion around the leading edge sharply, they have self-adjusting mechanisms regarding numerical viscosity and they also have robustness. The third feature more than compensates for the additional operations required.

ACKNOWLEDGEMENTS

The authors would like to express their sincere gratitude to Mr. Hajime Miyoshi, Director of the Computational Sciences Division of the National Aerospace Laboratory, for his advice and encouragement. In addition, this study has been done as a software package development in NAL.

REFERENCES

1. A. Harten, 'High resolution schemes for hyberbolic conservation laws', *J. Comput. Phys.*, **49,** 357–393 (1983).
2. A. Harten and S. Osher, 'Uniformly high-order accurate nonoscillatory schemes I', *SIAM J. Numer. Anal.*, **24,** 279–309 (1987).
3. A. Harten, B. Engquist, S. Osher and S. Chakravarthy, 'Uniformly high-accurate essentially nonoscillatory schemes III', *ICASE Report No. 86–22*, April 1986.
4. H. C. Yee, R. F. Warming and A. Harten, 'Implicit total variation diminishing (TVD) schemes for steady-state calculations', *J. Comput. Phys.*, **57,** 327–360 (1985).
5. H. C. Yee and A. Harten, 'Implicit TVD schemes for hyperbolic conservation laws in curvilinear coordinates', *AIAA paper 85–1513*, 1985.
6. S. R. Chakravarthy and S. Osher, 'A new class of high accuracy TVD schemes for hyperbolic conservation laws', *AIAA paper 85–0363*, 1985.
7. Y. Takakura, T. Ishiguro and S. Ogawa, 'On the recent difference schemes for the three-dimensional difference schemes', *AIAA paper 87–1151*, 1987.
8. T. H. Pulliam and D. S. Chaussee, 'A diagonal form of an implicit approximate factorization algorithm', *J. Comput. Phys.*, **39,** 347–363 (1981).
9. H. C. Yee and Y. C. Young, 'Numerical simulation of shock wave diffraction by TVD schemes', *AIAA paper 87–0112*, 1987.
10. S. Ogawa and T. Ishiguro, 'Numerical simulations of flow field with variable boundaries', *Preprint of ISCFD*, Tokyo, 1985, pp. 931–942.
11. R. Beam and R. F. Warming, 'An implicit finite difference algorithm for hyperbolic systems in conservation law form', *J. Comput. Phys.*, **22,** 87–110 (1976).
12. T. H. Pulliam and J. L. Steger, 'Recent improvements in efficiency, accuracy, and convergence for implicit approximate factorization algorithms', *AIAA paper 85–0360*, 1985.
13. P. L. Roe, 'Approximate Riemann solvers, parameter vectors, and difference schemes', *J. Comput. Phys.*, **43,** 357–372 (1981).
14. V. Schmitt and F. Charpin, 'Pressure distributions on the ONERA-M6 wing at transonic Mach numbers', *AGARD AR-138–B1*, 1979.
15. T. Ishiguro, 'Numerical analysis of transonic full potential flows about wings', *NAL TR-731*, 1982.
16. Y. Takakura, T. Ishiguro and S. Ogawa, 'On the difference schemes of the three-dimensionsl Euler equations', *Theor. Appl. Mech.*, **36,** 17–34 (1988).